Journal of Hydrology: Regional Studies 45 (2023) 101303

Contents lists available at ScienceDirect

Journal of Hydrology: Regional Studies

journal homepage: www.elsevier.com/locate/ejrh

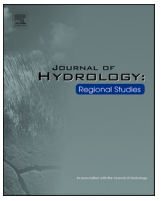

Spatiotemporal green water dynamics and their responses to variations of climatic and underlying surface factors: A case study in the Sanjiang Plain, China

Chi Xu [a,b,c], Wanchang Zhang [a,b,*], Shuhang Wang [d,**], Hao Chen [e,f], Abdullah Azzam [a,b,c], Bo Zhang [d], Yongxin Xu [g], Ning Nie [h]

[a] Key Laboratory of Digital Earth Science, Aerospace Information Research Institute, Chinese Academy of Sciences, Beijing 100094, China
[b] International Research Center of Big Data for Sustainable Development Goals, Beijing 100094, China
[c] University of Chinese Academy of Sciences, Beijing 100049, China
[d] National Engineering Laboratory for Lake Pollution Control and Ecological Restoration, Chinese Research Academy of Environmental Sciences, Beijing 100012, China
[e] Institute of Surface-Earth System Science, School of Earth System Science, Tianjin University, Tianjin 300072, China
[f] Critical Zone Observatory of Bohai Coastal Region, Tianjin University, Tianjin 300072, China
[g] Department of Earth Sciences, University of the Western Cape, Cape Town 7535, South Africa
[h] Key Laboratory of Geographic Information Science of the Ministry of Education, School of Geographic Sciences, East China Normal University, Shanghai 200241, China

ARTICLE INFO

Keywords:
Green water
Climatic and LULC changes
ESSI-3 model
Hydrological simulation
Remotely sensed information
Sanjiang Plain

ABSTRACT

Study region: The Sanjiang Plain (SJP), located at the confluence reaches of the Heilong, Songhua, and Wusuli Rivers in Northeast China.
Study focus: This study aimed to quantify the effects of varying climate and land-use/land-cover (LULC) dynamics on green water (GW) over the SJP during two distinctive periods (i.e., pre-2000 and post-2000), when synergetic effects of increased precipitation and temperature and rapid development of agriculture occurred. This assessment used the distributed eco-hydrological model ESSI-3. Multivariable and multi-objective calibration approaches (i.e., discharge, evapotranspiration, and terrestrial water storage anomaly) were used to ensure the high accuracies of the model outputs.
New hydrological insights for the region: This research concluded that GW flow and GW storage in the SJP evidently increased after 2000 compared with before. Across the SJP, GW flow and GW storage responded differently to climate changes and LULC dynamics during pre-2000 and post-2000 period. Our results demonstrated that GW storage changes were predominately affected by climatic changes, especially variations in precipitation, whose contribution accounted for more than 56% after 2000. However, GW flow changes were mainly governed by LULC changes, especially the influence of cropland transformation, whose contribution increased over 20% in the post-2000 period. This study posed a deep insight regarding impacts of regional climatic and

* Corresponding author at: Key Laboratory of Digital Earth Science, Aerospace Information Research Institute, Chinese Academy of Sciences, Beijing 100094, China.
** Corresponding author.
E-mail addresses: xuchi17@mails.ucas.ac.cn (C. Xu), zhangwc@radi.ac.cn (W. Zhang), wangsh@craes.org.cn (S. Wang), hao_chen@tju.edu.cn (H. Chen), Engr.AbdullahAzzam@mails.ucas.ac.cn (A. Azzam), zhangbo@craes.org.cn (B. Zhang), yxu@uwc.ac.za (Y. Xu), nnie@geo.ecnu.edu.cn (N. Nie).

https://doi.org/10.1016/j.ejrh.2022.101303
Received 26 October 2022; Received in revised form 3 December 2022; Accepted 10 December 2022
Available online 14 December 2022

LULC changes on GW dynamics, which may benefit decision-making for planting structure optimization and adjustment over the region.

1. Introduction

Water is the most valuable resource on our Earth (Degano et al., 2021). Water resources can be divided into blue water (BW) and green water (GW) (Quinteiro et al., 2018). GW refers to the water infiltrated by precipitation and stored in unsaturated soil layers (green water storage), and also refers to the actual evapotranspiration (ET) released into the atmosphere by the combination of soil evaporation and vegetation transpiration (green water flow) (Fisher et al., 2017; Ma et al., 2021). BW is freely flowing liquid water at the surface and in the subsurface layers, i.e., water in rivers, streams, and groundwater (Falkenmark and Rockström, 2006). Pioneer studies have reported that GW contributes significantly more to the human water consumption than BW at a global scale, especially for agricultural products (~87%) (Xie et al., 2020). Furthermore, comparisons of different models such as hydrological model, agricultural model and vegetation growth model reveal that GW utilization rate of global agricultural production is approximately four or five times higher than the BW utilization rate (Hoff et al., 2010). Thereby, GW is a vital water resource to support vegetation growth, especially in the rain-fed crop regions (Qiao et al., 2014; Velpuri et al., 2017).

It is an indisputable fact that the global warming has brought great pressure on agriculture water resources worldwide (Luan et al., 2018). Based on climate and socioeconomic changes, mid- and high-latitude regions will face greater agriculture water stresses in the 21st century, including greater regional disparities in the distribution of agriculture water availability and increased agricultural water requirements (Fabre et al., 2015). Both the IPCC (Intergovernmental Panel on Climate Change) and the FAO (Food and Agriculture Organization of the United Nations) have ranked agriculture as one of the most vulnerable sectors to climate change, especially for developing countries (Veettil et al., 2022). The increase of temperature with the increase of CO_2 and other greenhouse gas emissions as well as the frequent occurrence of extreme climate events under climate change pose a direct impact on the growth of crops, which will reduce the amount of agriculture water resources available and intensify the contradiction between crop water supply and demand (Azzam et al., 2022). Additionally, the transformation of LULC types, the adjustment of planting area and structure will also have a significant impact on agricultural water supply and water demand (Sivakumar, 2011; Mehrotra et al., 2013; Li et al., 2021). Thus, information regarding the quantity and spatial-temporal variations of regional and global GW and identification of its driving forces are fundamental needs for better understanding and managing regional ecosystem to ensure the safety of agricultural production, which have become emerging issues in the field of environmental studies (Jeyrani et al., 2021).

Hydrological models are helpful to quantitatively understand dynamics of GW variations and using them in conjunction with analyses of climate and LULC changes can provide essential information about the impacts of these factors on GW dynamics (Krysanova and White, 2015). The choice of model depends on the availability of data, the size of the problem, the characteristics of the study region, the desired spatial and temporal resolution, the degree of error allowed, the uncertainty of the simulation, and the robustness of the model (Faramarzi et al., 2017; Ma and Szilagyi, 2019; Ma and Zhang, 2022). Hydrological models such as SWAT (Soil and Water Assessment Tool) and VIC (Variable Infiltration Capacity) are usually used for such purposes. However, for the semi-distributed hydrological model SWAT, the hydrologic response unit (HRU) input approach of basic geographic data limits the comprehensive utilization of spatial distribution information of the driving data, such as the gridded meteorological data, and the gridded remotely sensed LULC and vegetation products (Liang et al., 1994; Chen et al., 2019b; Guiamel and Lee, 2020). As a fully distributed macroscale hydrological model, VIC predicts various temporal-spatial variations of surface processes at coarse resolutions in regional and continental scales but cannot simulate hydrological processes at high resolution (Zhang et al., 2021). In addition, the leaf area index (LAI) remains constant within one month and is kept stable for each month of a year, this oversimplification of crop growth constrains the VIC model in accurate simulations of vegetation transpiration and soil moisture estimations (Siad et al., 2019). Therefore, these hydrological models are not suitable for simulating the spatial distribution of hydrological components related to GW, and thus the simulated results can't be used to estimate the temporal and spatial difference of GW under climate and underlying surface changes.

As a physically-based distributed hydrological model that exploits spatially and temporally varying climate forcing and model-driven parameters on maximum, ESSI-3 (the third version of the infiltration Excess and Saturation excess Soil-water Integration model for hydrology) has demonstrated excellent performances in hydrological simulations of various watersheds with different catchment sizes under various climatic conditions (Zhang and Zhang, 2006; Xu et al., 2009; Chen et al., 2014; Liu et al., 2015; Chen and Zhang, 2019; Wang et al., 2022). It is worth emphasizing that preparation of reliable input model parameters is the essential step toward a dependable estimation of regional hydrology. The soil and vegetation parameterization methods commonly used in hydrological models are normally based on parameter lookup table. However, these static parameter values (e.g., LAI, soil hydraulic and thermal properties) determined by soil and LULC type data cannot adequately reflect the spatiotemporal heterogeneity, thus leading to additional uncertainties (Ma and Szilagyi, 2019; Ma et al., 2021). An advancement of the ESSI-3 model is that the soil- and vegetation-related parameters are typically based on globally or regionally oriented spatiotemporal soil characteristics and vegetation parameters products derived from several types of remotely sensed dataset. Based on the soil parameters (e.g., soil texture and bulk density) and pedotransfer functions (Dai et al., 2013), the grid-based soil hydraulic properties (e.g., saturated hydraulic conductivity, saturated water content, and permanent wilting point) can be obtained to ensure that the model simulation of evapotranspiration and soil moisture meets the accuracy requirements (Wang et al., 2022). In addition, considering the continuity of the vegetation growth process, a time dimensional approach is usually used to interpolate the long-term dynamic vegetation parameters like LAI to a daily

scale (Zhang and Zhang, 2006; Chen et al., 2018). Therefore, ESSI-3 model was adopted in this research to simulate the regional hydrological processes for better understanding the GW water resource partitioning and its dynamic changes.

Due to the unique natural conditions (e.g., flat terrain, fertile soil, suitable climate, and abundant water sources), the Sanjiang Plain (SJP) is suitable for the development of agriculture (Jin et al., 2016). After years of development and construction, the SJP has become the most important commercial grain production base and the key edible oil production base ensuring country's food security of China (Fu et al., 2020). However, rapid population growth and enhanced industrialization over the SJP in recent decades have led to enormous pressure in water resource partitioning for the key croplands and wetlands of the region (Hao et al., 2016). Owing to the excessive pursuit of economic benefits, the planting area of crops in the SJP has increased sharply, which makes the water resource shortage for agricultural purposes become severe day by day. Moreover, climate change has increased the occurrence frequency of extreme climate events, which pose serious impact on crop growth and alter the hydrological processes in the SJP region (Wang et al., 2011). Thus, it is essential to understand the current hydrological regime by evaluating the impacts of climate and underlying surface changes on hydrological processes of the region for water resource management and regional sustainable development.

As a microcosm of a water-scarce region, the water resource partitioning of the SJP is strongly influenced by climate and LULC changes, and the GW variations in response to these changes have drawn extensive attention due to the importance of GW in regional sustainability (Sun et al., 2022). Nevertheless, few knowledge about this issue is available from literature, especially regarding its insufficient and fragmented temporal and spatial information. Furthermore, some researches have addressed the influences of LULC changes on hydrology with focus mainly on the transition of land use from cropland to grassland due to its ecological function, while the influences of other LULC changes (i.e., wetland degradation) was ignored. Therefore, to quantitatively explore water resource partitioning for sustainable management policymaking across the SJP, a comprehensive study was conducted. Under the context of significant climatic change characterized by the increased precipitation and temperature as well as the enhanced anthropogenic activities represented by rapid development of agriculture, the study period (1985–2018) was divided into two periods: 1985–1999 and 2000–2018 (before and after 2000). This research mainly addressed the issues of the spatial-temporal variations of the GW dynamics at the whole region and pixel scale in the two distinctive periods. The isolated and combined impacts of climate and LULC changes on GW dynamics throughout the SJP and relative contributions of each LULC type and climate factor on GW variations were also systematically investigated.

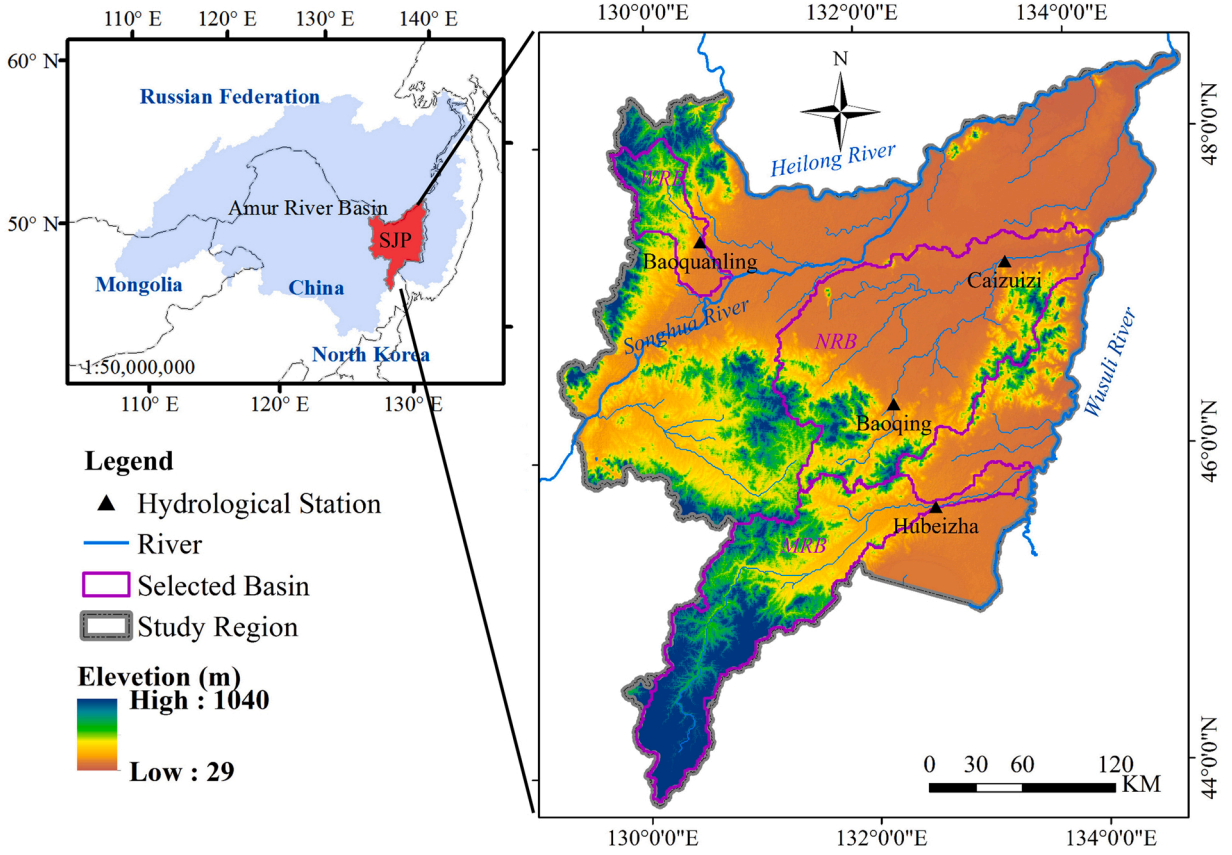

Fig. 1. The geographical location, geomorphology, river systems, and other relevant information of the SJP.

2. Materials and methods

2.1. Study area

Located in mid- and high-latitude region, the Sanjiang Plain (SJP) (43°49′55″−48°27′40″N, 129°11′20″−135°05′26″E) plays critical roles as a biodiversity region, a food production base, and an ecological security barrier in northeastern China (Fig. 1). The total area of this region is approximately 108,800 km^2, which accounts for about 21.6% of Heilongjiang Province. The terrain characteristic of the SJP is high in the southwest and low in the northeast. Three river systems, namely the Heilong, Songhua, and Wusuli Rivers, flow through the region, which is renowned as "a land of plenty" (Shi et al., 2015). The climate in the region is temperate humid and semi-humid continental monsoon climate, characterized by a rainy and humid summer and a cold and dry winter. The annual average temperature and precipitation are between 1.4 and 3.6 °C and 500–650 mm, respectively (Fu et al., 2020; Sun et al., 2022). The rainy season is mainly concentrated in summer and autumn, accounting for approximately 80% of the annual rainfall, lasting from June to September of a year. Abundant sunshine hours throughout the year ranging from 2400 to 2500 h and the average temperature varying from 21 °C to 22 °C in July grant this region rich of sunshine, rain, and heat in the same season and is suitable for the agricultural development, especially for crop production of high-quality rice, maize, and soybeans (Jin et al., 2016). Large-scale reclamation began in the 1950 s, and many large state-owned farms were set up successively till approximately 2000, making this region the largest agricultural reclamation area and a vital commercial grain production base in China (Fu et al., 2020).

2.2. Datasets

To set up the hydrological model, the detailed information of model input data (e.g., the data type, the duration of the datasets, the spatial and temporal resolution, the accessible website to download the specific dataset, and references) were presented in Table 1.

To calibrate and validate the hydrological model, datasets utilized from remote sensing, in-situ observations, and the Global Land Data Assimilation System land surface models were also obtained: (1) the observed discharge from four stations (as shown in Fig. 1) on three main tributaries were collected from the Hydrological yearbook of Heilongjiang and the Songhua River basin management organization for the period of 2007–2012; (2) three mascon-based GRACE (Gravity Recovery and Climate Experiment) products from the Jet Propulsion Laboratory (JPL-M), the Center for Space Research at University of Texas, Austin (CSR-M), and the Goddard Space Flight Center (GSFC-M) were provided by the GRACE Tellus website (please refer to Watkins et al., 2015, Save et al., 2016, and Loomis et al., 2019 for detailed descriptions of the JPL-M, CSR-M, and GSFC-M data, respectively, data available at https://grace.jpl.nasa.gov/); (3) gridded soil moisture storage (SMS), snow water equivalent (SWE), and total canopy water storage (CWS) simulations from GLDAS-2.1 two LSMs (Rodell et al., 2004), i.e., the VIC and Noah model were collected from https://disc.gsfc.nasa.gov/datasets/; (4) monthly remotely sensed MODIS evapotranspiration (MOD16A2) product (Mu et al., 2011) from 2000 to 2018 (data available at https://ladsweb.modaps.eosdis.nasa.gov/search/).

Table 1
Summary of the datasets utilized in this study to drive the ESSI-3 model.

Input Data	Details	Source	Resolution and Time	Reference
Meteorology	Wind speed Specific humidity Precipitation Air temperature Solar radiation Surface pressure	China Meteorological Forcing Dataset (CMFD) (http://data.tpdc.ac.cn/)	0.1°, daily, 1982–2018	He et al. (2020)
Soil property	Depth to bedrock Sand content Silt content Clay content Bulk density	SoilGrids250m (https://www.soilgrids.org/)	250 m, fixed	Hengl et al. (2017)
Vegetation parameter	Leaf area index (LAI)	GLOBMAP-based (https://zenodo.org/)	8 km, 16-day, 1982–2000, 8-day, 2001–2018	Liu et al. (2012)
	Land use and land cover (LULC)	Resources and Environment Data Cloud Platform (http://www.resdc.cn/)	1 km, year of 1980/ 1990/ 2000/2010/2018	RESDC data products
	Tree cover fraction	MODIS-based (https://lpdaac.usgs.gov/)	500 m, fixed	Kobayashi et al. (2016)
	Normalized difference vegetation index (NDVI)	GIMMS-based (http://ecocast.arc.nasa.gov/data/pub/gimms/) MODIS-based (https://lpdaac.usgs.gov/)	0.083°, 15-day, 1982–2000, 500 m, 8-day, 2001–2018	Tucker et al. (2005) MODIS data products
Others	DEM	SRTMDEM (http://www.gscloud.cn/)	90 m, fixed	Farr et al. (2007)

2.3. Methodology

2.3.1. ESSI-3 model

The distributed hydrological model ESSI-3 was set up to capture the spatial-temporal variability of hydrological processes of the SJP. Briefly, The ESSI-3 model, which is based on energy balance and water balance and constituted with various basic modules (e.g., a remote sensing-based ET module, a three-layer soil water balance module, and a groundwater module) and specific hydrological process modules (e.g., permafrost hydrology, snow melting, and wetland hydrology), can accurately characterize various hydrological fluxes (e.g., runoff and ET) and states (e.g., SWE, CWS, SMS, and groundwater storage) (Zhang and Zhang, 2006; Liu et al., 2015; Chen and Zhang, 2019; Wang et al., 2022). Especially for this study, based on a remote sensing-based two-leaf Jarvis-type canopy conductance model (RST-Gc), the actual ET is partitioned into four parts, including wet canopy evaporation (E^c_{wet}), saturated soil surface evaporation (E^c_{sat}), wet soil evaporation (E^c_{moi}), and dry canopy transpiration (E^c_{dry}). A three-layer soil water balance module incorporates the remote sensing-based ET module to simulate soil water content and water storage tension. Thus, the soil water storage of the ESSI-3 model is partitioned into three layers individual stores. The vertical root distribution information and oxygen stress of roots are also considered when the soil water content approaches saturation (Chen and Zhang, 2019). Mainly from the perspective of water balance, the groundwater component is integrated in the ESSI-3 model. The groundwater storage is considered based on a first-order linear reservoir approach and a simple groundwater model with recharge from the third soil layer, capillary rise, and discharge into streams (Wang et al., 2022). The groundwater consumption module (e.g., the groundwater withdrawal) is not considered in the model. As such, the groundwater component of ESSI-3 model is likely unsatisfactory due to the simplified generalization of the groundwater module. Additionally, the ESSI-3 model integrates remotely sensed data (e.g., LAI, NDVI, and tree cover fraction) and gridded soil products (e.g., SoilGrids250m data) to calibrate the soil and vegetation parameters. In conclusion, the modeling architecture considerably improves the simulation accuracies of spatially heterogeneous hydrological processes with time by inhibiting uncertainties in model structure and physical parameterizations.

GW flow, defined in this study, is the sum of actual evapotranspiration, and GW storage is defined as the ESSI-3 model output of water accumulated in the three soil moisture layers (including SWC_1, SWC_2, and SWC_3) (Falkenmark and Rockström, 2006; Zhao et al., 2016):

$$GWflow = E_a = E^c_{dry} + E^c_{Wet} + E^s_{Sat} + E^s_{Moi} \tag{1}$$

$$\mathrm{GWstorage} = \mathrm{SWC}_1 + \mathrm{SWC}_2 + \mathrm{SWC}_3 \tag{2}$$

where SWC_1, SWC_2, and SWC_3 is the soil water content in first, second, and third layer, respectively; E_a is the actual evapotranspiration.

In this study, ESSI-3 model simulations were conducted during the period 1982–2018, with the first three years serving as a warm-up period (the simulation results for the period of 1982–1984 is not considered in the following analysis) for balancing main hydrological component conditions such as soil and groundwater aquifers, and the remaining years being used for calibration and validation. Since the driving data input to the model had multiple spatial resolutions, the bilinear interpolation approach was used to generate grid datasets with a consistent spatial resolution (1 km) (Gao et al., 2018; Wang et al., 2022).

2.3.2. Model validation

The water yield of the SJP only accounts for a small part of the discharge through the mainstream of Heilong, Songhua, and Wusuli Rivers. Therefore, using the measured discharge from the mainstream is not appropriate for calibrating and validating the model (Wen et al., 2020). ESSI-3 model was calibrated and verified by using the measured discharge from four hydrologic stations on the representative tributaries of the Songhua River and Wusuli River in the study area. The geolocation of these river basins and the corresponding hydrological stations were presented in Fig. 1. Since daily observed discharge data were not available, the model calibration was performed at monthly scale. The main characteristics of these hydrometric stations and time periods of available streamflow data for model evaluation were shown in Table 2.

To evaluate model performance in evapotranspiration simulations, the ETMOD16 product sequence was used as reference data of actual evapotranspiration in this study. The MODIS Terrestrial ET product uses the Penman-Monteith equation to estimate the sum of the evaporation from wet and dry soil layers, the evaporation from canopy water retention, and the transpiration from plant leaves and stems (Mu et al., 2011; Kisi, 2016). Therefore, the MOD16A2 ET product was adopted to evaluate the actual evapotranspiration simulated by the ESSI-3 model.

SMS is a key state variable of the regional hydrological cycle. However, it is difficult to assess the accuracy of simulated SMS based on in-situ measurements owing to the scarcity of gauged stations (Gao et al., 2018). Thus, the terrestrial water storage (TWS) simulated

Table 2
Main characteristics of hydrometric stations and time periods of available streamflow data for model evaluation.

Station name	River	Drainage area (km^2)	Calibration period	Validation period
Baoqing	Naoli River	3689	2007–2009, monthly	2010–2012, monthly
Caizuizi	Naoli River	20556	2007–2009, monthly	2010–2012, monthly
Hubeizha	Muling River	16020	2007, 2009, monthly	2010–2012, monthly
Baoquanling	Wutong River	3633	2007–2009, monthly	2010–2012, monthly

in ESSI-3 model was evaluated as an alternative solution for SMS assessment. The GRACE-based TWS data were utilized to evaluate the performance of the ESSI-3 model in TWS simulations.

TWS is defined as all phases of water stored above and below the Earth's surface, including soil moisture, snow/ice, surface water, groundwater, and water contained in biomass (Chen et al., 2019b). In general, a change in TWS can be computed as:

$$\Delta TWS = \Delta SMS + \Delta GWS + \Delta CWS + \Delta SWE \tag{3}$$

where SMS is the soil moisture storage, SWE is the snow water equivalent, CWS is the total canopy water storage, GWS is the groundwater storage. ΔTWS simulated by ESSI-3 model can be computed as:

$$\Delta TWS_{ESSI3} = \Delta SWC_1 + \Delta SWC_2 + \Delta SWC_3 + \Delta GWS + \Delta CWS + \Delta SWE \tag{4}$$

where SWC_1, SWC_2, SWC_3, SWE, CWS, and GWS represent the first, second, and third layer of soil moisture storage, snow water equivalent, plant canopy water, and groundwater storage from ESSI-3 model, respectively. ΔTWS of the study region was estimated with the GRACE-based TWS. Monthly changes of the GRACE-based TWS dataset was made available since April 2002 (Tapley et al., 2004; Soni and Syed, 2015). Currently, different processing centers offer various ΔTWS series. However, no data series of ΔTWS was confirmed as the best in quality (Landerer et al., 2015). In the present study, JPL, CSR, and GSFC mascon solutions within the study region were extracted and compared to investigate ΔTWS from 2003 to 2016. In addition, the scaling factors were used to modify their corresponding mascon grids for better comparisons between the GRACE-based TWS and the ESSI-3 simulated ones. GRACE-based TWS were specifically computed relative to a timely mean baseline from Jan 2004 to Dec 2009 including every month of a year. For comparisons ESSI-3 simulated outputs against GRACE-based TWS, the baseline value over the 2004–2009 period of each simulated components was computed and subtracted from all time steps.

Three common evaluation indicators, i.e., the correlation coefficient (*R*), the Nash-Sutcliff efficiency (*NSE*), and the determination coefficient (R^2) (equations can be found in the study of Chen et al., 2019b) were calculated for model evaluation.

2.3.3. Establishment of climate and LULC scenarios

In order to quantitatively assess the green water response to climate and LULC changes, three scenarios were established by combining different climate periods and LULC conditions. Based on the changing tendency of climate and LULC (as shown in Section 3.2), the meteorological data were divided into two periods: the period of 1982–1999 and the period of 2000–2018, and the LULC map of 1980 and 2018 were selected to represent the LULC conditions during two periods (as shown in Fig. 2). By comparing the simulation results under different scenarios, the isolated and combined influences of climate change and LULC change on GW were quantitatively analyzed (as shown in Table 3). Based on the simulated results under these scenarios, the contributions of climate change and LULC change was estimated as follows:

$$\text{Contribution}_{C\ \text{lim ate}} = \frac{|S_2 - S_1|}{|S_2 - S_1| + |S_3 - S_2|} \times 100\% \tag{5}$$

$$\text{Contribution}_{LULC} = \frac{|S_3 - S_2|}{|S_2 - S_1| + |S_3 - S_2|} \times 100\% \tag{6}$$

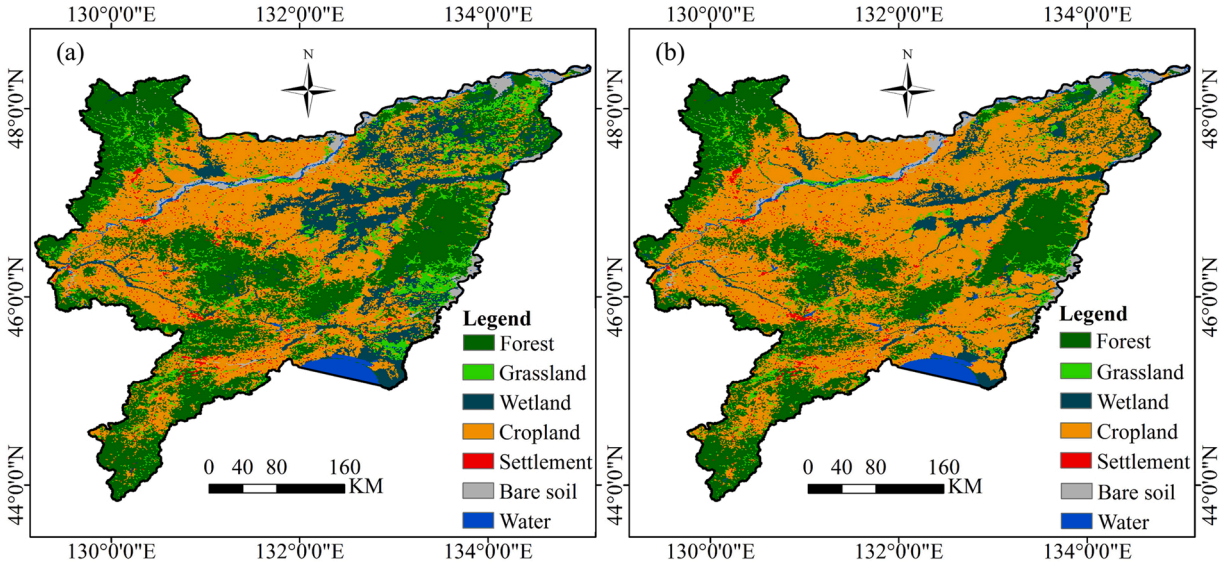

Fig. 2. Land use/cover distribution of year1980 (a) and 2018 (b) in SJP.

Table 3
The settings of different simulated scenarios.

Scenarios	Climate	LULC
S1	1982–1999	1980
S2	2000–2018	1980
S3	2000–2018	2018

2.3.4. Relative contributions of single climatic factor and LULC type

To explore the relative contribution of different LULC types, the contribution index proposed by Ahlström et al. (2015) was used to partition the contribution of each LULC class to the GW (Musavi et al., 2017). The contribution index (f_j) was expressed as:

$$f_j = \frac{\sum_t \frac{x_{jt}|X_t|}{X_t}}{\sum_t |X_t|} \tag{7}$$

$$X_t = \sum_j x_{jt} \tag{8}$$

where x_{jt} is the anomaly value for GW of grid j at time t (in years), and X_t is the anomaly value of GW in the whole region. The value of f_j ranges from − 1–1. Grid with higher and positive score means a greater contribution in governing GW.

To estimate the relative importance of different climatic factors (i.e., wind speed, pressure, relative humidity, precipitation, temperature and solar radiation) to GW changes, the LMG method was used. The LMG method identifies the direct contributions of a variable and its combined contributions with all other predictors (Fernández-Martínez et al., 2014). This measure has the important advantage that the results do not depend on the order of predictors in the model, as it clearly identifies nonlinear relationships between dependent and explanatory variables (Lee and Biggs, 2015). For details see Groemping (2006) and the R package "relaimpo_2.2–3" was us to calculate the LMG indicator (Groemping, 2006).

3. Results and discussions

3.1. Evaluation of model performance

Model calibration and verification for ESSI-3 model at four hydrological stations were shown in Table 4. The model performances for every selected subbasin were evaluated by *NSE* and R^2. The observed and simulated discharge at representative Caizuizi Station on the Naoli River, a tributary of the Wusuli River, and Baoquanling hydrological station on the Wutong River, a tributary of the Songhua River, are plotted in Fig. 3 for comparisons. For calibration and validation periods, model performance with R^2 of 0.82–0.92, and 0.81–0.83, and *NSE* of 0.77–0.89, and 0.74–0.83, respectively, suggested excellence of the ESSI-3 model in hydrological simulations in SJP.

Fig. 4 presents the spatial distribution of the correlation between ET_{ESSI3} and ET_{MOD16} from 2000 to 2018. It can be observed that correlation coefficients over larger than 96% of the study region were greater than 0.8. For those with relatively low correlation coefficients ($0.9 \geq R \geq 0.8$), cropland took the predominant land use type. MOD16 did not distinguish and parameterize C_3 and C_4 crops, which may result in a relatively low correlation between ET_{ESSI3} and ET_{MOD16} for those regions. In contrast, the different parameterization schemes for evapotranspiration estimation from C_3 and C_4 crops in the ESSI-3 model were specifically designed. Therefore, the evapotranspiration simulated by the ESSI-3 model was more refined and close to the actual conditions. For these grids shown in blue with low correlation coefficients ($R \leq 0.5$), the underlying surface type is mainly rivers. There is no doubt that water surface evaporation based on remote sensing estimation and model simulation will have large errors. The blank grids are due to the special treatment of some special areas (e.g., cities, ice and snow, and water bodies) in the MOD16 dataset.

Fig. 5 shows the monthly TWSA derived from the three mascon solutions, the ESSI-3 model and two LSM models (VIC model and Noah model). The simulated result of ESSI-3 model exhibited a high consistency over the period of 2003–2016 with those GRACE-based solutions. As shown in Table 5, for the TWSA simulated by the ESSI-3 and GRACE-derived, the results indicated a high agreement with *R* ranging from 0.65 to 0.69 ($p < 0.01$) for the period of 2003–2016. GRACE-derived TWSA and monthly scale VIC and Noah model simulation also showed a similar trends in terrestrial water storage, with the correlation coefficients of 0.65–0.70, and

Table 4
Statistics of *NSE* and R^2 at four hydrological stations in the calibration (2007–2009) and validation (2010–2012) periods.

Hydrological stations	R^2		*NSE*	
	Calibration	Validation	Calibration	Validation
Baoqing	0.82	0.81	0.77	0.74
Caizuizi	0.87	0.81	0.83	0.80
Hubeizha	0.85	0.82	0.79	0.75
Baoquanling	0.92	0.83	0.89	0.83

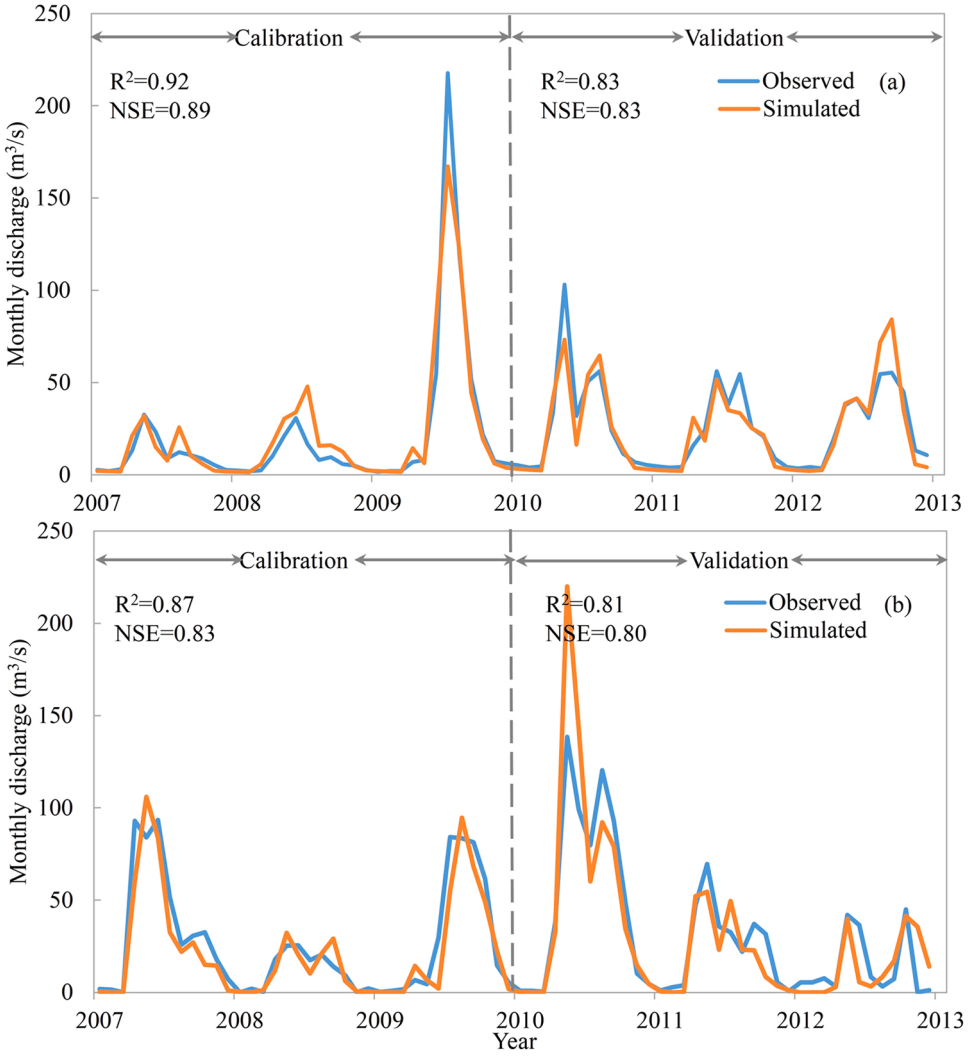

Fig. 3. Comparison of the measured and simulated discharge during the calibration (2007–2009) and validation (2010–2012) periods at two gauge stations: (a) the Baoquanling Station, and (b) the Caizuizi Station.

from 0.71 to 0.75 ($p < 0.01$), respectively. Although the long-term trend agreement between GRACE-derived TWSA and ESSI-3, NOAH, and VIC model simulations was at a high level, the differences appeared mostly in amplitude. It can be observed that the ESSI-3 model presented the better fit with GRACE observations with the smaller variation difference amplitude of TWSA. The performance of VIC, NOAH, and ESSI-3 model was measured by *NSE* ranging − 0.96–0.05, − 2.64 to − 0.49, and 0.33–0.47, respectively. The primary reason for this phenomenon was that anthropogenic activities were not considered in the VIC, NOAH, and ESSI-3 model, and the intensive agriculture irrigation and groundwater extraction in SJP put enormous pressure on TWS, especially the groundwater. Additionally, water storage components provided by Noah and VIC just included SWE, CWS, and SMS. NOAH and VIC models belong to LSMs, thus the groundwater storage component is not included (Chen et al., 2019b). However, the groundwater storage component is included in ESSI-3 model to better characterize the water balance. With respect to the monthly amplitude, this difference highlighted that the NOAH and VIC model was obviously underestimated or overestimated of TWSA relative to ESSI-3 model owing to the lack of groundwater storage component. Thus, variations in various hydrological states (e.g., soil moisture storage component) obtained from ESSI-3 model can better describe the dynamic characteristics of water storage components, although the ESSI-3 model doesn't take terrestrial water storage changes caused by anthropogenic factors such as groundwater extraction into account.

In summary, despite some uncertainties existed in hydrological simulations for specific seasons, the ET, SMS, TWS, and runoff were all simulated with satisfactory precision. This demonstrated the superiority of model simulations in producing various hydrological fluxes and states and laid the foundation for further estimating hydrological processes and investigating their variations and potential influencing factors.

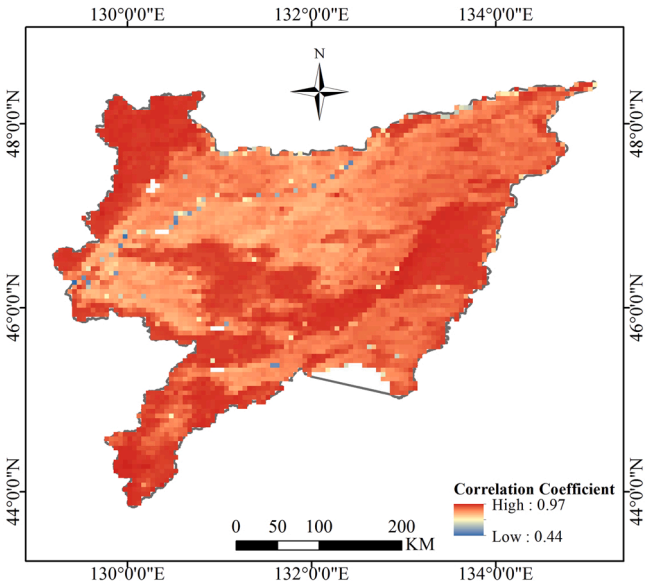

Fig. 4. Correlation coefficient between ET_{ESSI3} and ET_{MOD16} during 2000–2018.

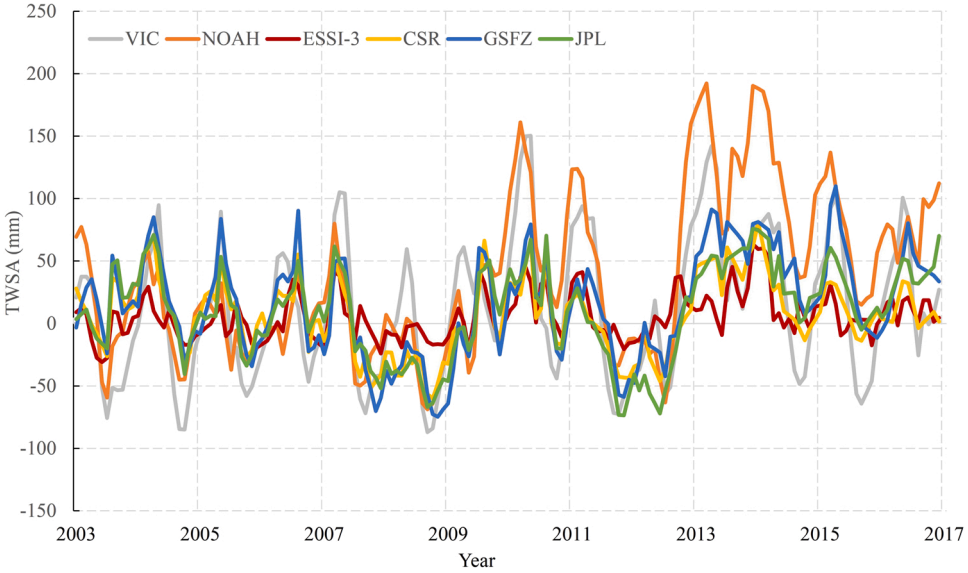

Fig. 5. Monthly TWSA series derived from the three GRACE solutions, and the simulations with two LSM models (VIC model and Noah model), as well as with ESSI-3 during the period of 2003–2016. Anomalies refer to the period 2004–2009.

Table 5
Correlation analysis of TWSA between three mascon solutions derived and the estimated from the simulations with different models for the period of 2003–2016.

	Nash-Sutcliff efficiency			Correlation Coefficient		
	CSR	GSFZ	JPL	CSR	GSFZ	JPL
VIC	-0.96	0.05	-0.34	0.69	0.7	0.65
NOAH	-2.64	-0.49	-1.01	0.71	0.71	0.75
ESSI-3	0.47	0.33	0.39	0.69	0.65	0.65

3.2. Climate and LULC changes analysis

To detect the temporal variations of climate factors in the SJP, the Mann–Kendall test was employed to examine the trends and abrupt changes of the temperature, and precipitation from 1985 to 2018 at the confidence level of 95%. Fig. 6a-d presented the area-averaged annual climate factors and Mann–Kendall Z value over the study region. The mean annual temperature and precipitation over the SJP varied with an increased rate during the study period. The sequential Mann–Kendall tests for the annual precipitation, as illustrated in Fig. 6c, indicated an apparent abrupt change in 2005, meanwhile several abrupt changes occurred from 2000 to 2005 in temperature, which suggested a significant abrupt change of climate factors took place around 2000–2005 over the SJP.

Fig. 7 exhibits the areas and ratios of seven primary land use/cover types from 1980 to 2018 over the SJP. In the year 1980, cropland, forest, and wetland took the predominant land use/cover types, accounting for approximately 36.05%, 34.93%, and 14.32% of the total area of the SJP, respectively. To the year 2018, land use/cover types changed dramatically with approximately 50.76% of the SJP changed to cropland, 31.98% forest and 6.68% the wetland. The agricultural land increased rapidly from 1980 to 2018, primarily due to the conversion of wetland and grassland.

To quantitatively investigate the change trend and LULC transformation among preliminary LULC types in the SJP, the LULC transformations during 5 specific periods (i.e., the period of 1980–1990, 1990–2000, 2000–2010, 2010–2018 and 1980–2018) were calculated, and the results are shown in Fig. 8. For the period from 1980 to 2018, the most significant area changes in the positive direction (increasing trend) were cropland, while the opposite cases were grassland and wetland. In the period of 1980–1990, the fastest area decreasing rate occurred in wetland, followed by grassland, with a decreasing rate of − 28.10% and − 13.51%, respectively. From 1990–2000, the fastest area decreasing took place in grassland, followed by wetland, with a decreasing rate of − 44.06% and − 21.69% respectively. The area increasing rate for cropland in these two periods was approximately15.80%, and 16.05%, respectively. For the two periods of 2000–2010 and 2010–2018, less area changes were found for all LULC types except for wetlands. These results also suggested that the 2000 can be taken as a turning year subject to the abrupt changes in LULC over the SJP.

In summary, to reasonably explain the dynamic influences of the climate change and LULC change across the SJP, scenarios studies between pre- and post-2000 were conducted for the purpose.

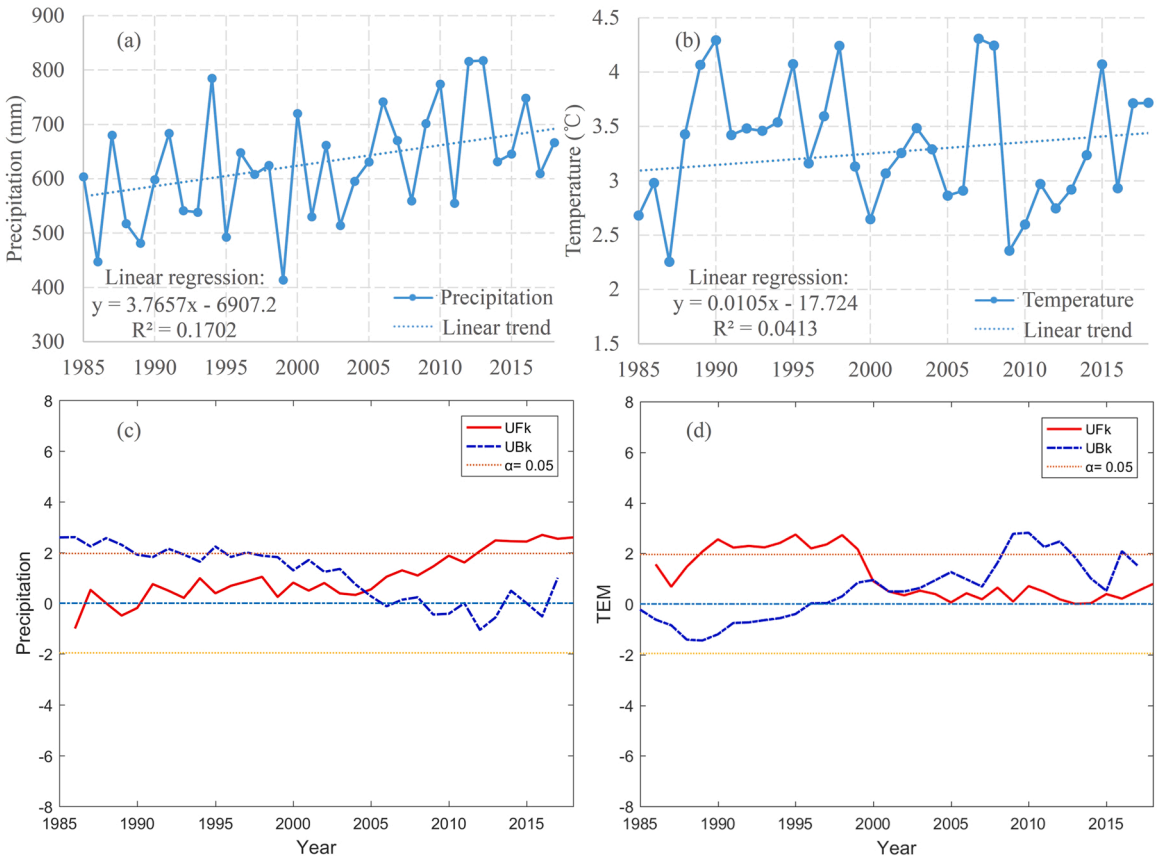

Fig. 6. Temporal changes of the area-averaged annual precipitation (a), temperature (b), and sequential Mann–Kendall tests for the annual precipitation (c) and temperature (d) with the forward-trend UFk and backward-trend UBk in the SJP during 1985–2018.

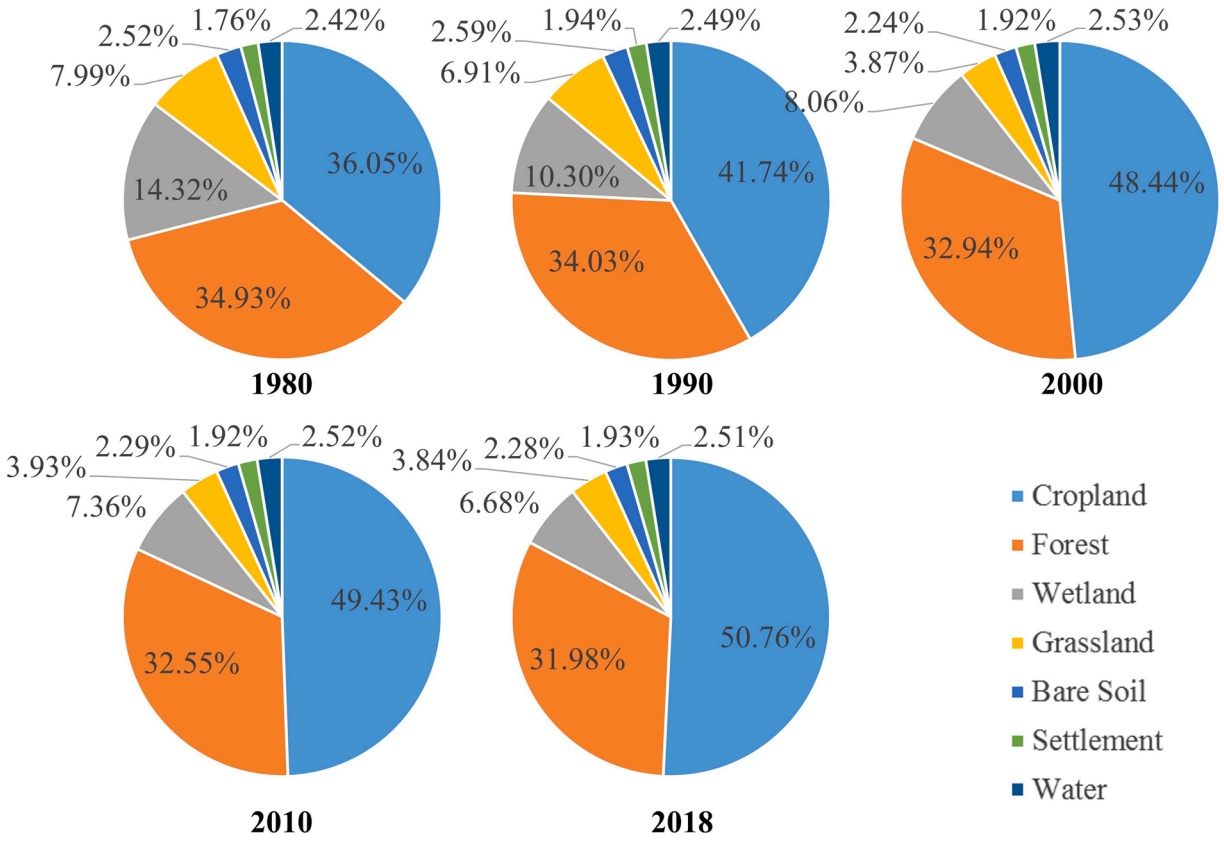

Fig. 7. The proportions of each LULC types during 1980–2018 over the SJP.

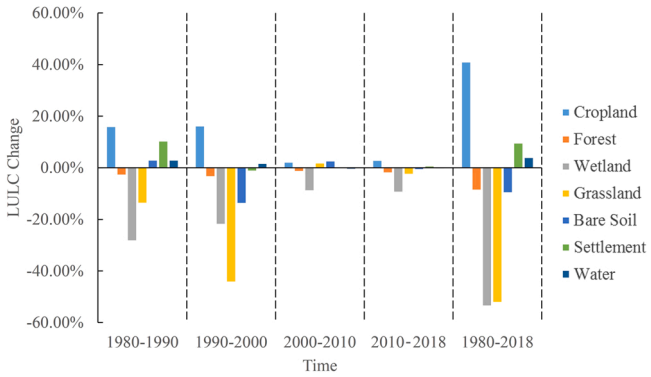

Fig. 8. Areal change rate (%) per 10 years for each LULC types over the SJP for study period.

3.3. The spatial-temporal variations of the GW flow and storage in the SJP

Fig. 9 plots the area-averaged annual GW flow and GW storage estimated from the simulated hydrological processes with ESSI-3 model over the SJP from 1985 to 2018. Generally, relative higher GW flow and GW storage can be observed for the post-2000 period compared with the pre-2000 period. The averaged GW flow and GW storage were 319.8 mm and 479.3 mm in pre-2000 period but slightly increased to 323.9 mm and 485.9 mm in post-2000 period, respectively.

Fig. 10 shows the spatial patterns of the trend significance computed at the 95% significance level for time series GW flow and GW storage images under the influence of climate change and LULC change. As exhibited in Fig. 10 a-b, apparent spatial heterogeneity for the changes of GW flow and GW storage from 1985 to 2018 over the SJP was carefully investigated. The results indicated that about 50.84% of the study region showed an increasing tendency in terms of GW flow, in which approximately 23.13% tended to increase significantly ($p < 0.05$), where the most obvious increasing trend occurred in the southeast and northeast region of the SJP. On the

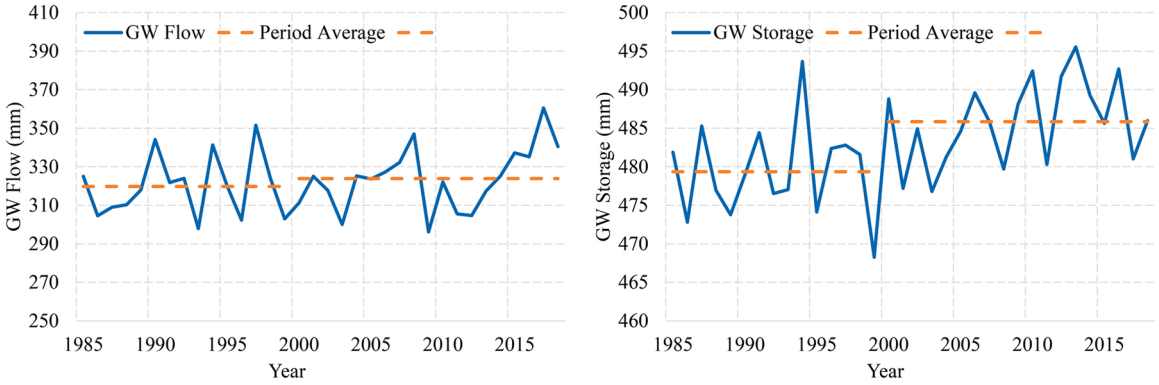

Fig. 9. Temporal changes of area-averaged annual GW flow and GW storage in the SJP during 1985–2018.

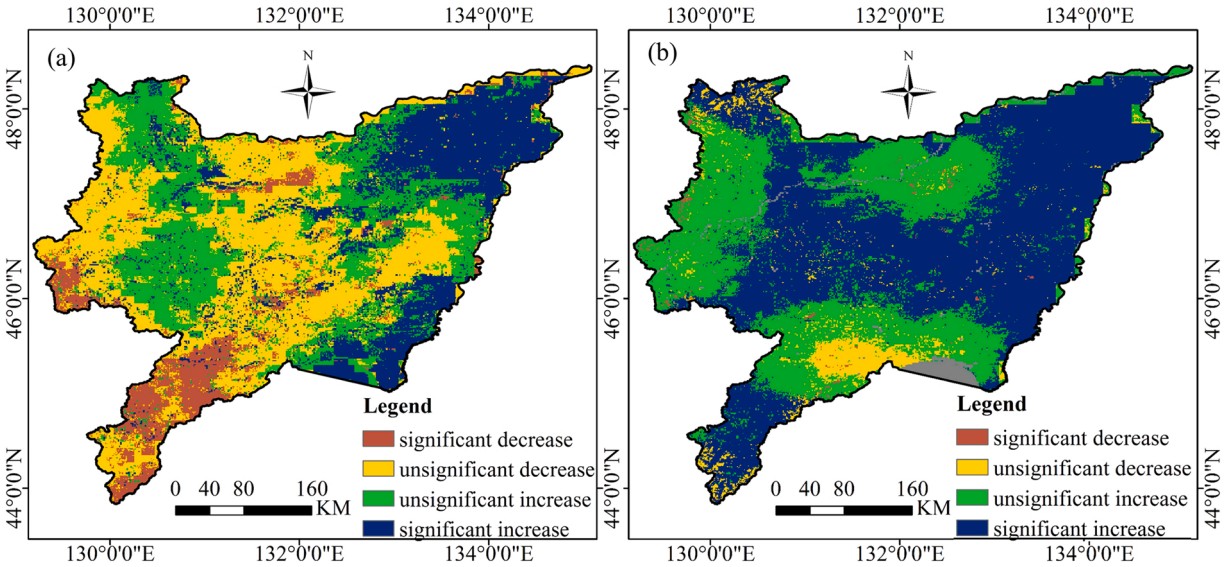

Fig. 10. Spatial patterns of the significance of changes for the annual GW flow (a), and GW storage (b) from 1985 to 2018 in the SJP.

contrary, a decreasing trend in GW flow was significant over about 10.16% of the SJP area, where the most significant reductions in GW flow were mainly distributed in the southwestern SJP area. Over past 34 years in the SJP, 91.25% of the total study area had exhibited an increasing trend in GW storage, and pixels with a significant increasing trend accounted for about 55.21%.

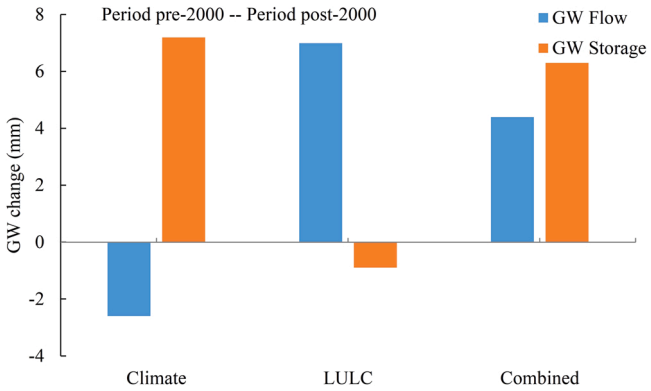

Fig. 11. The isolated and combined influences of climate change and LULC change, on GW flow and GW storage across the whole SJP during the period pre-2000 and post-2000.

3.4. Impacts of climate and LULC changes on GW flow and GW storage

3.4.1. Across the SJP

Fig. 11 demonstrates GW changes under the individual impact of climate change and LULC change, as well as their combined effects for the whole SJP during the period of pre-2000 and post-2000. GW flow increased by 4.4 mm considering the combined impacts of climate change and LULC change. This increase was predominantly attributable to LULC changes, which resulted in a 7 mm increase of GW flow, while climate change contributed − 2.6 mm decrease of GW flow in the opposite direction. The GW storage also increased by 6.3 mm under the combined influences of climate and LULC changes. A 7.2 mm increase of the GW storage was donated from the climate change, while a − 0.9 mm decrease of the GW storage was attributed to LULC change. The results revealed that the GW flow and GW storage changes responding to climate and LULC changes differed considerably during the period of pre-2000 and post-2000 throughout the SJP. The GW flow increased with a principal contribution from the LULC change, while the increase in GW storage was mainly influenced by climate change. Moreover, opposite responses of GW flow to climate changes as well as the GW storage to LULC changes were found during the period of pre-2000 and post-2000. The influence of climate change on GW flow was negative and climate change had a positive influence on GW storage, which was opposed to the influence of LULC change.

The isolated influence of climate change and LULC change to GW flow and storage changes at pixel scale were also estimated. To clarify, if the contribution of either climate or LULC exceeded 50% to a single pixel, this factor would be considered as the dominant factor governing the responses of either the GW flow or the GW storage for this pixel.

As illustrated in Fig. 12, 53% of the GW flow changes at pixel scale was attributed to climate change during the periods of pre-2000 and post-2000, which emphasized that the GW flow change had a high sensitivity to climate change. It also should be emphasized that in the majority (33%) of these pixels, the GW flow response to climate change were negative. For the remaining pixels, 46% of the GW flow variations were largely due to LULC change. Moreover, the spatial distribution of dominant factor that governed the GW flow change exhibited highly scale-dependent as observed in the whole SJP. Although more than half of these pixels (54%) were affected by climate change, LULC change still took the positive and predominant effect on the GW flow change in general, which implied that the positive and negative impacts induced by the climate change could offset each other and weakened their impacts at the whole SJP scale.

For the responses of GW storage to either climate or LULC change and their joint effect, the climate change contributed about 95% GW storage change at pixel scale (with 89% positively and 6% negatively), while LULC change contributed only 5% to the GW storage change over the remaining regions, suggesting that climate change was the main factor controlling GW storage changes in SJP.

A noteworthy point was that GW flow under climate warming showed a decreasing during the period of pre-2000 and post-2000 (as shown in Fig. 11). Climate warming undoubtedly increased the rate of soil moisture evaporation and vegetation transpiration (Azzam et al., 2022). However, due to the general weakening of solar radiation and wind speed, the measured water surface evaporation at most meteorological and hydrological stations in China was decreasing, which also inhibited vegetation transpiration (Wang et al., 2018). The increase of CO_2 concentration also reduced the opening of leaf stomata and increased the resistance, which was also an important factor to curb vegetation transpiration. Besides, related studies showed that the calculated potential evapotranspiration of crop was also decreasing for the SJP (Ren et al., 2019). On the other hand, the prolongation of plant growth period and the increase of biomass caused by climate warming would also increase water consumption (Zhou et al., 2021). However, the plant growth period set in ESSI-3 model for this study was constant. Therefore, GW flow (i.e., actual evapotranspiration) of farmland and ecosystem simulated by ESSI-3 model decreased after climate warming. This founding also emphasized that whether the actual evapotranspiration of different regions and different crops increased or decreased after climate warming still needed to be measured and studied.

3.4.2. Dominant factors governing the GW flow and GW storage changes

Since LULC changes took the predominant role governing the GW flow changes over the SJP, the impact of each LULC type on GW flow were further assessed in spite of the climate change effects. Using the contribution of land use/cover change to GW flow as an indicator to reveal the relationship between the land use/cover changes and the GW flow at different geographical locations and time. According to statistics of LULC changes in the SJP in different time of study period in Section 3.2, the significant land use conversion took place around 2000 with rapid area expansion of cropland and the shrinkage of forest, grassland and wetland. So the contributions of these four main land use types (i.e., cropland, forest, grassland, and wetland) were distinguished. The relative contribution rates for the remaining LULC types, such as water, settlement, and bare soil, were not shown due to the small proportion of the study region.

Fig. 13 presents each land use type and corresponding ratio to GW flow change during the period of pre-2000 and post-2000 across the SJP. Before 2000, cropland contributed 37.64% to the GW flow change of the entire SJP, followed by forest (31.79%), wetland (17.67%) and grassland (9.92%). After 2000, the contribution of cropland exerted significantly to 58.84%, while contributions of both wetland and grassland dropped to 5.85% and 4.16%, respectively, but the forest remained stable. This result was similar to the historical LULC conversion patterns occurred in SJP, where the majority of wetland and grassland was replaced by cropland during the period of pre-2000 and post-2000.

Since climate change was the main factor controlling GW storage change, the impacts of each climatic factor and corresponding ratio to GW storage change during the period of pre-2000 and post-2000 across the SJP were investigated as presented in Fig. 14. Before 2000, the relative contribution of precipitation to GW storage variation across the SJP was 42.42%, followed by solar radiation (22.09%), relative humidity (11.39%), and wind speed (10.13%). After 2000, the contribution of precipitation significantly increased to 56.80%, followed by temperature (11.39%) and relative humidity (10.13%). The results indicated that precipitation remained the most important factor dominating GW storage change. In addition, because of the processes that simulated fluxes and water storage change occurred in soil aquifer, climatic factors such as relative humidity and radiation, which dominated changes in

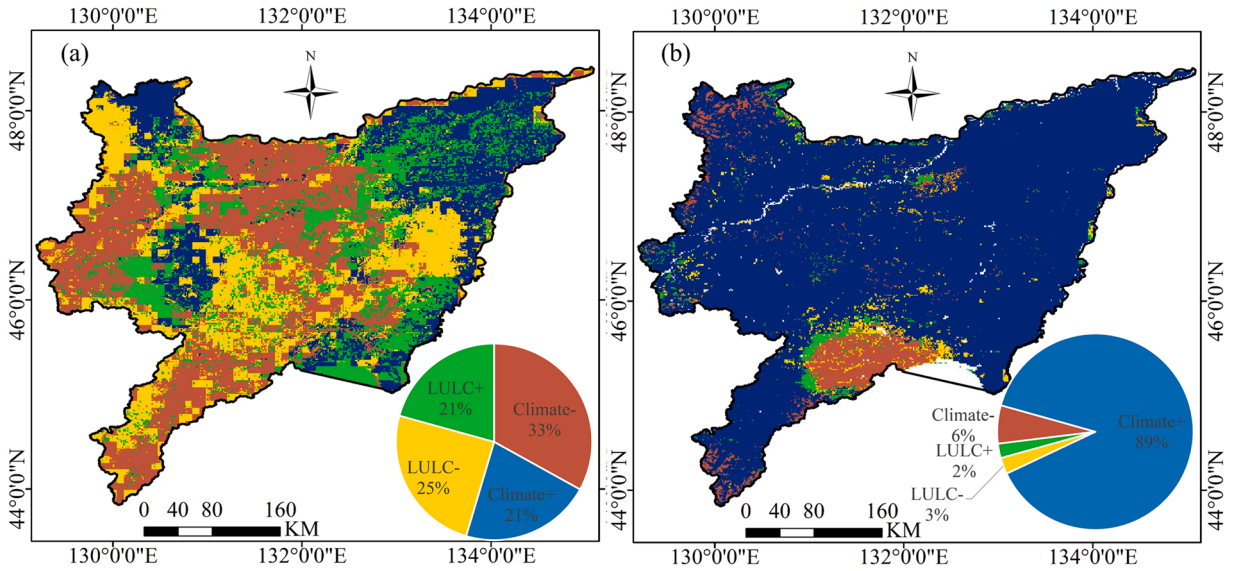

Fig. 12. The leading factor controlling the GW flow change (a) and GW storage change (b) at the pixel scale in SJP. + /− indicated the positive/ negative effects on GW flow and storage changes. The pie chart showed dominant factor types and corresponding ratios.

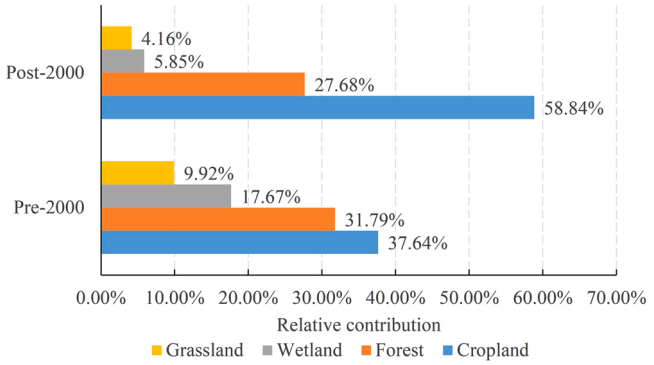

Fig. 13. The relative contributions of different LULC to the GW flow changes at pixel scale for the whole SJP.

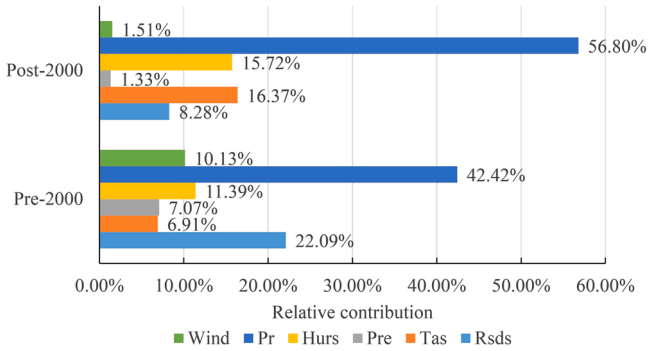

Fig. 14. The impacts of each climatic factor and corresponding ratio to GW storage change for the whole SJP in the studied period. Abbreviations: Wind, wind speed; Pr, pressure; Hurs, relative humidity; Pre, precipitation; Tas, temperature; Rsds, solar radiation.

evapotranspiration and runoff components, also affected soil hydrological processes. Therefore, this study also highlighted the importance of these factors to GW storage.

3.5. Hydrological modelling uncertainty and limitations

Traditionally, the hydrological models commonly use the single streamflow data for the model calibration and validation. Though this single evaluation approach is still being widely used around hydrological assessment, more efforts have emphasized that a comprehensive calibration strategy (e.g., intermediate gauges, checking for additional variables and considering their spatial distribution, not just at a specific point, etc.) can achieve a better model performance (Puertes et al., 2019; Wen et al., 2020).

In this study, two other water balance terms were selected for model validation. Firstly, GW flow, which represented actual evapotranspiration, was carefully investigated. The ETMOD16 product series were used as a reference to evaluate the model's performance in evapotranspiration simulation. The MOD16A2 product provides actual evapotranspiration estimates from the land surface which can be useful to evaluate the actual evapotranspiration simulated by the model. Additionally, for GW storage representing soil moisture, the model performance in the terrestrial soil moisture components simulations was carefully checked by comparing the results from the GRACE solutions, the LSMs and ESSI-3 model outputs, and the results suggested that ESSI-3 model could effectively simulate the composition of GW.

Yet, ample space remained to improve some limitations that should be considered in the future in present study. First, because of the existing multi-spatial resolutions input gridded datasets, there was only a simplest method, the bilinear interpolation method, was used to downscale the coarse resolution climatic forecasts to fine resolution. More advanced spatial downscaling approaches (e.g., multilinear regression method, random forests method, artificial neural network method) are suggested to be employed in the future studies for spatial performance improvement (Gao et al., 2018). Fortunately, the satisfactory performance of the ESSI-3 simulations of various hydrological processes over the SJP ensured the present studies on the GW flow and storage. Second, only five LULC maps that represented the underline condition of the SJP for specific periods were applied for simulations and the followed studies in the present study. Since LULC change is a dynamic process rather than abrupt change (Chen et al., 2019a), it is recommended to use more land-use maps for better characterization of LULC dynamics in further studies. Thirdly, this study did not consider the effects of other anthropogenic activities (e.g., irrigation withdrawals, reservoir regulation) and topographic changes (e.g., terrain and slope), which were also significant driving factors in governing hydrological response to LULC changes (Wang et al., 2022).

4. Conclusions

In this study, the ESSI-3 model was set up to assess the influences of climate and LULC changes on GW in the SJP of China. The excellent capability of ESSI-3 model was confirmed by the strong correlations between the observed and simulated discharges, the MODIS-based and simulated evaporation, the GRACE-based and simulated TWSA. Simulations showed that the combined effects of climate and LULC changes increased GW flow by 4.4 mm and increased GW storage by 6.3 mm during the period of pre-2000 and post-2000, whereas GW flow and GW storage responded differently to climate and LULC changes. Climate change decreased GW flow by − 2.6 mm and increased GW storage by 7.2 mm, while LULC change had an opposite effect on GW flow (increased by 7 mm) and GW storage (decreased by −0.9 mm). Although LULC change had a greater impact on GW flow than climate change for the whole SJP, climate change altered GW flow to a greater extent than LULC change for the pixel scale, accounting for 54% of the region. Moreover, climate change played a more important role in GW storage for across the region and at pixel scale. Further analysis suggested that the contribution of cropland on GW flow exerted significantly from 37.64% to 58.84% during the period of pre-2000 and post-2000, and the contribution of precipitation on GW storage increased from 42.42% before 2000–56.80% after 2000.

Although the hydrological modeling process in this study seems well represent the spatiotemporal distribution of green water, there are some limitations associated with the study remain to be solved in future study, especially for the uncertainty from input data (e.g., precipitation and temperature). The original spatial resolution of CMFD dataset is still coarse (0.1°) for regional study, and the data downscaling process from coarse resolution to fine resolution (1 km) are unsatisfactory without combining various environmental variables to improve the accuracy and enhance the spatial information. This implies that additional downscaling methods (e.g., statistical downscaling methods) need to be applied to obtain accurate high spatiotemporal gridded data.

This study can be used as a useful guideline for similar research to investigate the temporal and spatial pattern change and trend on green water under climate and LULC changes. The findings of this study combined with related researches on crop water requirements can provides a scientific basis for suitable cultivation planning program and agricultural water management for crop production in SJP, especially for rain-fed crops.

CRediT authorship contribution statement

Chi Xu: Conceptualization, Methodology, Software, Data curation, Formal Analysis, Writing – original draft. **Wanchang Zhang:** Conceptualization, Supervision, Writing – review & editing. **Shuhang Wang:** Methodology, Writing – review & editing. **Hao Chen:** Methodology, Software, Data curation, **Abdullah Azzam:** Writing – review & editing. **Bo Zhang:** Data curation, **Yongxin Xu:** Formal Analysis, **Ning Nie:** Writing – review & editing.

Declaration of Competing Interest

The authors declare that they have no known competing financial interests or personal relationships that could have appeared to influence the work reported in this paper.

Data Availability

Data will be made available on request.

Acknowledgments

The authors are grateful to the National Tibetan Plateau Data Center (http://data.tpdc.ac.cn), the GRACE mascon data from all the agencies, i.e. JPL, CSR, and GSFC (http://grace.jpl.nasa.gov, http://www2.csr.utexas.edu/grace, and https://earth.gsfc.nasa.gov), and the Goddard Earth Sciences Data and Information Services Center (GES DISC) for providing datasets. This study is jointly financed by the Key R & D and Transformation Program of Qinghai Province [Grant No. 2020-SF-C37] and the National Natural Science Foundation of China [Grant No. 42101034]. The authors appreciate the editor-in-chief and two anonymous reviewers for their valuable comments and suggestions that helped improve the manuscript.

Appendix A. Supporting information

Supplementary data associated with this article can be found in the online version at doi:10.1016/j.ejrh.2022.101303.

References

Ahlström, A., Raupach, M.R., Schurgers, G., et al., 2015. The dominant role of semi-arid ecosystems in the trend and variability of the land CO_2 sink. Science 348, 895–899. https://doi.org/10.1126/science.aaa1668.

Azzam, A., Zhang, W., Akhtar, F., et al., 2022. Estimation of green and blue water evapotranspiration using machine learning algorithms with limited meteorological data: a case study in Amu Darya River Basin, Central Asia. Comput. Electron. Agric. 202, 107403 https://doi.org/10.1016/j.compag.2022.107403.

Chen, H., Zhang, W., 2019. Variations of simulated water use efficiency over 2000-2016 and its driving forces in Northeast China. Proc. SPIE. https://doi.org/10.1117/12.2533127.

Chen, H., Zhang, W., Gao, H., et al., 2018. Climate change and anthropogenic impacts on wetland and agriculture in the songnen and Sanjiang Plain, Northeast China. Remote Sens. 10. https://doi.org/10.3390/rs10030356.

Chen, H., Zhang, W., Jafari Shalamzari, M., 2019a. Remote detection of human-induced evapotranspiration in a regional system experiencing increased anthropogenic demands and extreme climatic variability. Int. J. Remote Sens. 40, 1887–1908. https://doi.org/10.1080/01431161.2018.1523590.

Chen, H., Zhang, W., Nie, N., et al., 2019b. Long-term groundwater storage variations estimated in the Songhua River Basin by using GRACE products, land surface models, and in-situ observations. Sci. Total Environ. 649, 372–387. https://doi.org/10.1016/j.scitotenv.2018.08.352.

Chen, Z., Zhang, W., Yan, C., 2014. Application of ESSI distributed hydrological model in Huaihe River Basin. J. China Hydrol. 34, 17–24.

Dai, Y., Shangguan, W., Duan, Q., et al., 2013. Development of a China dataset of soil hydraulic parameters using pedotransfer functions for land surface modeling. J. Hydrometeorol. 14, 869–887. https://doi.org/10.1175/JHM-D-12-0149.1.

Degano, M.F., Rivas, R.E., Carmona, F., et al., 2021. Evaluation of the MOD16A2 evapotranspiration product in an agricultural area of Argentina, the Pampas region. Egypt. J. Remote Sens. Space Sci. 24, 319–328. https://doi.org/10.1016/j.ejrs.2020.08.004.

Fabre, J., Ruelland, D., Dezetter, A., et al., 2015. Simulating past changes in the balance between water demand and availability and assessing their main drivers at the river basin scale. Hydrol. Earth Syst. Sci. 19, 1263–1285. https://doi.org/10.5194/hess-19-1263-2015.

Falkenmark, M., Rockström, J., 2006. The new blue and green water paradigm: breaking new ground for water resources planning and management. J. Water Resour. Plan. Manag. 132, 129–132. https://doi.org/10.1061/(ASCE)0733-9496(2006)132:3(129).

Faramarzi, M., Abbaspour, K.C., Adamowicz, W.L., et al., 2017. Uncertainty based assessment of dynamic freshwater scarcity in semi-arid watersheds of Alberta, Canada. J. Hydrol.: Reg. Stud. 9, 48–68. https://doi.org/10.1016/j.ejrh.2016.11.003.

Farr, T.G., Rosen, P.A., Caro, E., et al., 2007. The shuttle radar topography mission. Rev. Geophys. 45. https://doi.org/10.1029/2005RG000183.

Fernández-Martínez, M., Vicca, S., Janssens, I.A., et al., 2014. Nutrient availability as the key regulator of global forest carbon balance. Nat. Clim. Change 4, 471–476. https://doi.org/10.1038/nclimate2177.

Fisher, J.B., Melton, F., Middleton, E., et al., 2017. The future of evapotranspiration: global requirements for ecosystem functioning, carbon and climate feedbacks, agricultural management, and water resources. Water Resour. Res. 53, 2618–2626. https://doi.org/10.1002/2016WR020175.

Fu, J., Liu, J., Wang, X., et al., 2020. Ecological risk assessment of wetland vegetation under projected climate scenarios in the Sanjiang Plain, China. J. Environ. Manag. 273, 111108 https://doi.org/10.1016/j.jenvman.2020.111108.

Gao, H., Zhang, W., Chen, H., 2018. An improved algorithm for discriminating soil freezing and thawing using AMSR-E and AMSR2 soil moisture products. Remote Sens. 10. https://doi.org/10.3390/rs10111697.

Groemping, U., 2006. Relative importance for linear regression in R: the package relaimpo. J. Stat. Softw. 17, 1–27. https://doi.org/10.18637/jss.v017.i01.

Guiamel, I.A., Lee, H.S., 2020. Watershed modelling of the Mindanao River Basin in the Philippines using the SWAT for water resource management. Civ. Eng. J. 6, 626–648. https://doi.org/10.28991/cej-2020-03091496.

Hao, X., Li, P., Han, X., et al., 2016. Effects of free-air CO_2 enrichment (FACE) on N, P and K uptake of soybean in northern China. Agric. For. Meteorol. 218, 261–266. https://doi.org/10.1016/j.agrformet.2015.12.061.

He, J., Yang, K., Tang, W., et al., 2020. The first high-resolution meteorological forcing dataset for land process studies over China. Sci. Data 7, 25. https://doi.org/10.1038/s41597-020-0369-y.

Hengl, T., Mendes De Jesus, J., Heuvelink, G.B.M., et al., 2017. SoilGrids250m: global gridded soil information based on machine learning. PLOS ONE 12, e0169748. https://doi.org/10.1371/journal.pone.0169748.

Hoff, H., Falkenmark, M., Gerten, D., et al., 2010. Greening the global water system. J. Hydrol. 384, 177–186. https://doi.org/10.1016/j.jhydrol.2009.06.026.

Jeyrani, F., Morid, S., Srinivasan, R., 2021. Assessing basin blue–green available water components under different management and climate scenarios using SWAT. Agric. Water Manag. 256, 107074 https://doi.org/10.1016/j.agwat.2021.107074.

Jin, X., Du, J., Liu, H., et al., 2016. Remote estimation of soil organic matter content in the Sanjiang Plain, Northest China: the optimal band algorithm versus the GRA-ANN model. Agric. For. Meteorol. 218–219, 250–260. https://doi.org/10.1016/j.agrformet.2015.12.062.
Kisi, O., 2016. Modeling reference evapotranspiration using three different heuristic regression approaches. Agric. Water Manag. 169, 162–172. https://doi.org/10.1016/j.agwat.2016.02.026.
Kobayashi, T., Tsend-Ayush, J., Tateishi, R., 2016. A new global tree-cover percentage map using MODIS data. Int. J. Remote Sens. 37, 969–992. https://doi.org/10.1080/01431161.2016.1142684.
Krysanova, V., White, M., 2015. Advances in water resources assessment with SWAT—an overview. Hydrol. Sci. J. 60, 771–783. https://doi.org/10.1080/02626667.2015.1029482.
Landerer, F.W., Wiese, D.N., Bentel, K., et al., 2015. North Atlantic meridional overturning circulation variations from GRACE ocean bottom pressure anomalies. Geophys. Res. Lett. 42, 8114–8121. https://doi.org/10.1002/2015GL065730.
Lee, R.M., Biggs, T.W., 2015. Impacts of land use, climate variability, and management on thermal structure, anoxia, and transparency in hypereutrophic urban water supply reservoirs. Hydrobiologia 745, 263–284. https://doi.org/10.1007/s10750-014-2112-1.
Li, X., Zhang, Y., Ma, N., et al., 2021. Contrasting effects of climate and LULC change on blue water resources at varying temporal and spatial scales. Sci. Total Environ. 786, 147488 https://doi.org/10.1016/j.scitotenv.2021.147488.
Liang, X., Lettenmaier, D.P., Wood, E.F., et al., 1994. A simple hydrologically based model of land surface water and energy fluxes for general circulation models. J. Geophys. Res. Atmosph. 99, 14415–14428. https://doi.org/10.1029/94JD00483.
Liu, Y., Liu, R., Chen, J.M., 2012. Retrospective retrieval of long-term consistent global leaf area index (1981–2011) from combined AVHRR and MODIS data. J. Geophys. Res. Biogeosci. 117. https://doi.org/10.1029/2012JG002084.
Liu, Y., Zhang, W., Zhang, Z., 2015. A conceptual data model coupling with physically-based distributed hydrological models based on catchment discretization schemas. J. Hydrol. 530, 206–215. https://doi.org/10.1016/j.jhydrol.2015.09.049.
Loomis, B.D., Luthcke, S.B., Sabaka, T.J., 2019. Regularization and error characterization of GRACE mascons. J. Geod. 93, 1381–1398. https://doi.org/10.1007/s00190-019-01252-y.
Luan, X.B., Yin, Y.L., Wu, P.T., et al., 2018. An improved method for calculating the regional crop water footprint based on a hydrological process analysis. Hydrol. Earth Syst. Sci. 22, 5111–5123. https://doi.org/10.5194/hess-22-5111-2018.
Ma, N., Szilagyi, J., 2019. The CR of evaporation: a calibration-free diagnostic and benchmarking tool for large-scale terrestrial evapotranspiration modeling. Water Resour. Res. 55, 7246–7274. https://doi.org/10.1029/2019WR024867.
Ma, N., Zhang, Y., 2022. Increasing Tibetan Plateau terrestrial evapotranspiration primarily driven by precipitation. Agric. For. Meteorol. 317, 108887 https://doi.org/10.1016/j.agrformet.2022.108887.
Ma, N., Szilagyi, J., Zhang, Y., 2021. Calibration-free complementary relationship estimates terrestrial evapotranspiration globally. e2021WR029691 Water Resour. Res. 57. https://doi.org/10.1029/2021WR029691.
Mehrotra, R., Sharma, A., Kumar, D.N., et al., 2013. Assessing future rainfall projections using multiple GCMs and a multi-site stochastic downscaling model. J. Hydrol. 488, 84–100. https://doi.org/10.1016/j.jhydrol.2013.02.046.
Mu, Q., Zhao, M., Running, S.W., 2011. Improvements to a MODIS global terrestrial evapotranspiration algorithm. Remote Sens. Environ. 115, 1781–1800. https://doi.org/10.1016/j.rse.2011.02.019.
Musavi, T., Migliavacca, M., Reichstein, M., et al., 2017. Stand age and species richness dampen interannual variation of ecosystem-level photosynthetic capacity. Nat. Ecol. Evol. 1, 0048. https://doi.org/10.1038/s41559-016-0048.
Puertes, C., Lidón, A., Echeverría, C., et al., 2019. Explaining the hydrological behaviour of facultative phreatophytes using a multi-variable and multi-objective modelling approach. J. Hydrol. 575, 395–407. https://doi.org/10.1016/j.jhydrol.2019.05.041.
Qiao, L., Hong, Y., Mcpherson, R., et al., 2014. Climate change and hydrological response in the trans-state Oologah Lake watershed–evaluating dynamically downscaled NARCCAP and statistically downscaled CMIP3 simulations with VIC model. Water Resour. Manag. 28, 3291–3305. https://doi.org/10.1007/S11269-014-0678-Z.
Quinteiro, P., Rafael, S., Villanueva-Rey, P., et al., 2018. A characterisation model to address the environmental impact of green water flows for water scarcity footprints. Sci. Total Environ. 626, 1210–1218. https://doi.org/10.1016/j.scitotenv.2018.01.201.
Ren, X., Li, H., Zhang, Y., et al., 2019. Water requirement characteristics and influencing factors of main crops in the Sanjiang Plain from 2000 to 2015. Arid Land. Geography 42, 854–866. https://doi.org/10.12118/j.issn.1000-6060.2019.04.17.
Rodell, M., Houser, P.R., Jambor, U., et al., 2004. The global land data assimilation system. Bull. Am. Meteorol. Soc. 85, 381–394. https://doi.org/10.1175/BAMS-85-3-381.
Save, H., Bettadpur, S., Tapley, B.D., 2016. High-resolution CSR GRACE RL05 mascons. J. Geophys. Res. Solid Earth 121, 7547–7569. https://doi.org/10.1002/2016JB013007.
Shi, F., Song, C., Zhang, X., et al., 2015. Plant zonation patterns reflected by the differences in plant growth, biomass partitioning and root traits along a water level gradient among four common vascular plants in freshwater marshes of the Sanjiang Plain, Northeast China. Ecol. Eng. 81, 158–164. https://doi.org/10.1016/j.ecoleng.2015.04.054.
Siad, S.M., Iacobellis, V., Zdruli, P., et al., 2019. A review of coupled hydrologic and crop growth models. Agric. Water Manag. 224, 105746 https://doi.org/10.1016/j.agwat.2019.105746.
Sivakumar, B., 2011. Global climate change and its impacts on water resources planning and management: assessment and challenges. Stoch. Environ. Res. Risk Assess. 25, 583–600. https://doi.org/10.1007/s00477-010-0423-y.
Soni, A., Syed, T.H., 2015. Diagnosing land water storage variations in major Indian river basins using GRACE observations. Glob. Planet. Change 133, 263–271. https://doi.org/10.1016/j.gloplacha.2015.09.007.
Sun, Q., Xu, C., Gao, X., et al., 2022. Response of groundwater to different water resource allocation patterns in the Sanjiang Plain, Northeast China. J. Hydrol.: Reg. Stud. 42, 101156 https://doi.org/10.1016/j.ejrh.2022.101156.
Tapley, B.D., Bettadpur, S., Ries, J.C., et al., 2004. GRACE measurements of mass variability in the Earth system. Science 305, 503–505. https://doi.org/10.1126/science.1099192.
Tucker, C.J., Pinzon, J.E., Brown, M.E., et al., 2005. An extended AVHRR 8–km NDVI dataset compatible with MODIS and SPOT vegetation NDVI data. Int. J. Remote Sens. 26, 4485–4498. https://doi.org/10.1080/01431160500168686.
Veettil, A.V., Mishra, A.K., Green, T.R., 2022. Explaining water security indicators using hydrologic and agricultural systems models. J. Hydrol. 607, 127463 https://doi.org/10.1016/j.jhydrol.2022.127463.
Velpuri, N.M., Senay, G.B., 2017. Partitioning evapotranspiration into green and blue water sources in the conterminous United States. Sci. Rep. 7, 6191. https://doi.org/10.1038/s41598-017-06359-w.
Wang, L., Huo, A., Wang, J., et al., 2018. Impact of climate change on change of groundwater recharge based on SWAT model. Open J. Nat. Sci. https://doi.org/10.12677/OJNS.2018.63028.
Wang, S., Xu, C., Zhang, W., et al., 2022. Human-Induced water loss from closed inland Lakes: hydrological simulations in China's Daihai lake. J. Hydrol. 607, 127552 https://doi.org/10.1016/j.jhydrol.2022.127552.
Wang, Z., Song, K., Ma, W., et al., 2011. Loss and fragmentation of marshes in the Sanjiang Plain, Northeast China, 1954–2005. Wetlands 31, 945. https://doi.org/10.1007/s13157-011-0209-0.
Watkins, M.M., Wiese, D.N., Yuan, D.-N., et al., 2015. Improved methods for observing Earth's time variable mass distribution with GRACE using spherical cap mascons. J. Geophys. Res. Solid Earth 120, 2648–2671. https://doi.org/10.1002/2014JB011547.
Wen, S., Su, B., Wang, Y., et al., 2020. Comprehensive evaluation of hydrological models for climate change impact assessment in the Upper Yangtze River Basin, China. Clim. Change 163, 1207–1226. https://doi.org/10.1007/s10584-020-02929-6.

Xie, P., Zhuo, L., Yang, X., et al., 2020. Spatial-temporal variations in blue and green water resources, water footprints and water scarcities in a large river basin: a case for the Yellow River basin. J. Hydrol. 590, 125222 https://doi.org/10.1016/j.jhydrol.2020.125222.

Xu, J., Zhao, J., Zhang, W., et al., 2009. Mid-short-term daily runoff forecasting by ANNs and multiple process-based hydrological models. IEEE Youth Conf. Inf. Comput. Telecommun. 2009, 526–529. https://doi.org/10.1109/YCICT.2009.5382440.

Zhang, D., Zhang, W., 2006. Distributed hydrological modeling study with the dynamic water yielding mechanism and RS/GIS techniques. Proc. SPIE. https://doi.org/10.1117/12.690016.

Zhang, Y., Wu, Z., Singh, V.P., et al., 2021. Simulation of crop water demand and consumption considering irrigation effects based on coupled hydrology-crop growth model. e2020MS002360 J. Adv. Model. Earth Syst. 13. https://doi.org/10.1029/2020MS002360.

Zhao, A., Zhu, X., Liu, X., et al., 2016. Impacts of land use change and climate variability on green and blue water resources in the Weihe River Basin of northwest China. CATENA 137, 318–327. https://doi.org/10.1016/j.catena.2015.09.018.

Zhou, S., Zhang, W., Wang, S., et al., 2021. Spatial–temporal vegetation dynamics and their relationships with climatic, anthropogenic, and hydrological factors in the Amur River Basin. Remote Sens. 13 https://doi.org/13.10.3390/rs13040684.